

## Effect of spin-density waves on the lattice dynamics of lead

X. M. Chen and A. W. Overhauser

*Department of Physics, Purdue University, West Lafayette, Indiana 47907*

(Received 14 December 1988)

The phonon spectrum of Pb, first determined by Brockhouse *et al.* in 1962, exhibits large depressions in both longitudinal and transverse modes at the zone-boundary points  $\{100\}$ . The origin of this behavior has remained unclear. We show that a possible explanation involves the existence of a cubic family of small-amplitude spin-density waves (SDW's), having wave vectors  $\{\mathbf{Q}\}$  at each of the twelve  $\{211\}$ , or alternatively  $\{210\}$ , superlattice points. Each SDW causes a peak in the conduction-electron charge response function  $\chi(\mathbf{q})$  near the points  $\mathbf{q}=\pm\mathbf{Q}$ . SDW's have built-in charge modulations, equal in magnitude but opposite in sign, for both spin states. Only a small shift in the spatial phase  $\delta\phi=\epsilon\sigma_z$ , depending on the spin  $\sigma_z$ , creates an additional charge response for  $\mathbf{q}$  near  $\pm\mathbf{Q}$ . When this spin-split-phase contribution to  $\chi(\mathbf{q})$  is incorporated into the theory for the phonon spectrum, the anomalous behavior at  $\{100\}$  can be understood.

### I. INTRODUCTION

There has been a challenge for more than 25 years to understand the lattice dynamics of lead, which is one of the most complicated members of the simple-metal group. Beginning with the work of Toya<sup>1</sup> and of Vosko *et al.*,<sup>2</sup> many attempts have been made to explain Pb's phonon dispersion curves. Pseudopotential calculations have been less successful for Pb than for Al or alkali metals. Models which fit some phonon frequencies fail to reproduce other features in the spectrum.<sup>3-8</sup> Imaginary phonon frequencies are often found in calculations using Heine-Abarenkov pseudopotentials<sup>9</sup> or Harrison's first-principle scheme,<sup>10</sup> as well as with other models.<sup>3,8</sup>

In attempts to remedy the poor agreement between theory and experiment, investigators have included additional effects in their calculations, such as a third-order perturbation correction to the electron-ion pseudopotential,<sup>11,12</sup> conduction-electron-core exchange, nonlocal pseudopotentials,<sup>10</sup> relativistic spin-orbit interaction,<sup>13</sup> and effective electron-mass corrections.<sup>14</sup> However, the results remain unsatisfactory. Recently, Wang and Overhauser<sup>15</sup> pointed out that vibrations of the (last-filled)  $5d$  electron shell play an important role in the lattice dynamics of lead. Accordingly they introduced a dynamic pseudopotential and found phonon dispersion curves in fair agreement with experimental data. But the frequency dips near the  $\{100\}$  zone-boundary points remained unexplained.

Compared with other fcc metals the phonon spectrum of Pb is so peculiar that even a 26-parameter Born-von Kármán fit<sup>16</sup> (including eight neighbor shells) does not suffice. An analysis in terms of interplanar force constants indicated that measurable forces extend to distances greater than 20 Å (17th neighbor).<sup>17</sup> This conclusion does not depend on small features in the dispersion curves (such as Kohn anomalies), but primarily on the frequency dips near  $\{100\}$  mentioned above.

To the best of our knowledge, there is as yet no qualitative explanation for the frequency dips (in both longitudinal

and transverse modes) near  $\{100\}$ . Distortions of the Fermi surface from a free-electron shape<sup>18</sup> seem to be too minor to be relevant. Another possibility is that the normal plane-wave ground state of an electron gas is not suitable for Pb. In this paper we investigate the possible consequences of a spin-density-wave (SDW) structure on lattice dynamics.

It is well known that in the Hartree-Fock approximation an interacting electron gas always tends to have a SDW state.<sup>19,20</sup> Static sinusoidal modulations of spin-up and spin-down electron densities are then exactly out of phase. As we will show below, the charge response of a SDW state is quite different from that of a normal plane-wave state. A spin-split-phase mechanism, developed by Giuliani and Overhauser<sup>21</sup> for the spin response of a CDW state, allows an external charge perturbation, having a spatial periodicity close to that of the SDW, to create a phase shift between spin-up and spin-down charge modulations. This phase shift causes a charge response which adds to the ordinary Lindhard response of an electron gas. As a consequence small peaks in the electronic dielectric function  $\epsilon(\mathbf{q})$ , arise for  $\mathbf{q}$  near  $\pm\mathbf{Q}$ , where  $\mathbf{Q}$  is the SDW wave vector. We will show that this modification of  $\epsilon(\mathbf{q})$  can explain the observed anomalies in the phonon spectrum of Pb.

We shall assume the existence of a cubic family of SDW's in lead and shall employ the dynamic pseudopotential theory for phonon spectra recently developed by Wang and Overhauser<sup>22</sup> (hereafter referred to as WO). The SDW families we shall consider are three SDW's with  $\mathbf{Q}=\{100\}$ , six SDW's with  $\mathbf{Q}=\{110\}$ , twelve SDW's with  $\mathbf{Q}=\{210\}$ , and twelve SDW's with  $\mathbf{Q}=\{211\}$ . The last alternative would be the *a priori* choice since  $|\mathbf{Q}_{211}|=0.987(2k_f)$ , a value close to  $2k_f$ , the Fermi surface diameter, as required by the SDW instability theorem.<sup>20</sup>

It turns out that the first two choices mentioned above fail to provide an explanation of the frequency anomalies. However the last two choices for the SDW family can account for the frequency depressions near  $\{100\}$  in both

longitudinal and transverse branches.

The plan of the paper is as follows. In Sec. II the spin-split-phase mechanism is described and shown to cause an extra charge response of a SDW state. In Sec. III the core-shell exchange energy is discussed, and its role in lattice dynamics is introduced. In Sec. IV, WO theory is reviewed and extended to include both the effects of the SDW's and the core-shell exchange energy. In Sec. V the phonon spectrum of lead is calculated for several SDW families and compared with experiment. Brief conclusions and remarks are presented in Sec. VI.

## II. CHARGE RESPONSE OF A SDW STATE

Let us first consider the jellium model of an ion-electron system. In the Hartree-Fock approximation the ground state of the system, in general, is a mixed SDW-CDW state characterized by modulated spin-up and spin-down electron densities<sup>23</sup>

$$n_{\sigma_z}(\mathbf{r}) = \frac{n}{2} [1 + p \cos(\mathbf{Q} \cdot \mathbf{r} + \phi_0 + \sigma_z \phi)], \quad (1)$$

where  $\sigma_z$  is the usual Pauli spin variable,  $n$  is the average density of the electron gas, and  $p$  is the fractional modulation of each charge density.  $\phi_0$  is an arbitrary phase which exhibits the translational degeneracy of the state.  $\phi$  is the so-called spin-split phase and plays a very important role in our discussion. The single-particle self-consistent potential felt by electrons in the state described by Eq. (1) is

$$V(\mathbf{r}, \sigma_z) = -G [\cos \phi \cos(\mathbf{Q} \cdot \mathbf{r} + \phi_0) - \sigma_z \sin \phi \sin(\mathbf{Q} \cdot \mathbf{r} + \phi_0)], \quad (2)$$

where  $G$  is the resulting energy-gap parameter. It is easy to see the relation of  $\phi$  to the charge distribution of the state: For  $\phi=0$  one has a pure CDW; for  $\phi=\pi/2$  one has a pure SDW. The spin response of a pure CDW state, incorporating a shift  $\delta\phi$  of a spin-split phase, was developed by Giuliani and Overhauser.<sup>21</sup> In this section we employ the same mechanism to discuss the charge response of a *pure* SDW state.

For a pure SDW state, the first term in the single-particle potential of Eq. (2) is zero. The remaining spin-dependent term produces spin-up and spin-down densities which are exactly 180° out of phase. The total electron density of a SDW state is uniform, as shown in Fig. 1(a). Suppose we now impose an external potential  $\delta V$ , having a wave vector  $\mathbf{q}$  equal to that of the SDW, e.g.,

$$\delta V(\mathbf{r}) = \delta V_Q \cos(\mathbf{Q} \cdot \mathbf{r} + \phi_Q), \quad (3)$$

where  $\phi_Q$  is the phase of the perturbation. This *spin-independent* perturbation will induce a small spin-split phase  $\delta\phi$ . Consequently the extra shift between spin-up and spin-down modulations will introduce a small total electron-density modulation, as shown in Fig. 1(b),

$$\begin{aligned} \delta n(\mathbf{r}) &= -np \sin(\delta\phi) \cos(\mathbf{Q} \cdot \mathbf{r} + \phi_0) \\ &\cong -np \delta\phi \cos(\mathbf{Q} \cdot \mathbf{r} + \phi_0). \end{aligned} \quad (4)$$

In the deformable jellium model the positive-ion back-

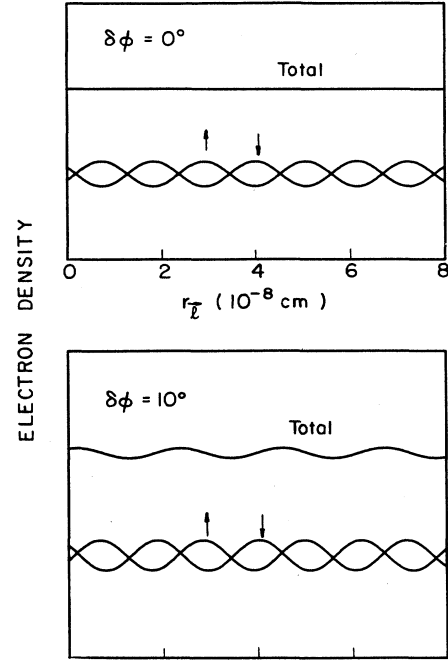


FIG. 1. Total spin-up, and spin-down electron densities vs spatial coordinate  $r_{\parallel}$  ( $\hat{T}$  is parallel to  $\mathbf{Q}$  of the SDW). (a) Spin-split phase  $\delta\phi=0$ ; (b) spin-split phase  $\delta\phi=10^\circ$ .

ground will introduce a compensating charge modulation so as to maintain microscopic neutrality of the system. In a real metal, however, the positive ions are not perfectly free to move. In order to study the spin-split-phase response, we shall now take the ions to be fixed at their lattice sites. The change in energy (per unit volume) resulting from the perturbation (3) can be written (after integration over  $\mathbf{r}$ ) as

$$\Delta E_{\text{tot}} = -\frac{1}{2} np \delta V_Q \delta\phi \cos(\phi_Q - \phi_0) + \Delta E_{\text{ssp}}. \quad (5)$$

The first term is the interaction energy of the perturbation (3) with the induced electron density (4).  $\Delta E_{\text{ssp}}$  is the energy increase of the electron gas caused by the presence of the spin-split phase  $\delta\phi$ . Two terms contribute to it. The first one is the Coulomb energy  $\Delta E_s$  of  $\delta n(\mathbf{r})$  with itself, which equals  $\pi e^2 n^2 p^2 (\delta\phi)^2 / Q^2$ . The second is the change in electronic correlation energy  $\Delta E_c$  caused by the relative shift of up- and down-spin densities. This latter effect was evaluated by Giuliani and Overhauser.<sup>21</sup> Accordingly,

$$\begin{aligned} \Delta E_{\text{ssp}} &= \Delta E_s + \Delta E_c \\ &= \frac{\pi e^2}{Q^2} n^2 p^2 (\delta\phi)^2 - \Delta E_{c\uparrow\downarrow}^{\text{CDW}} [\cos(2\delta\phi) - 1] \\ &\cong \kappa^2 (\delta\phi)^2 + 2 \Delta E_{c\uparrow\downarrow}^{\text{CDW}} (\delta\phi)^2, \end{aligned} \quad (6)$$

where  $\kappa^2 \equiv \pi e^2 n^2 p^2 / Q^2$ , and  $\Delta E_{c\uparrow\downarrow}^{\text{CDW}}$ , a negative quantity, is the correlation energy contribution of a pure CDW<sup>21</sup> caused by virtual scattering of antiparallel-spin pairs. (There are no shifts in exchange energy resulting from the

relative displacement of up- and down-spin electron distributions.) Notice that the correlation energy contribution in Eq. (6) tends to lower the energy. It follows that  $\kappa^2 > 2|\Delta E_{c\uparrow\downarrow}^{\text{CDW}}|$  for a metal with a stable SDW state.

Upon substituting Eq. (6) into Eq. (5), and minimizing  $\Delta E_{\text{tot}}$ , the equilibrium condition is

$$\delta\phi = \frac{np\delta V_Q \cos(\phi_Q - \phi_0)}{4(\kappa^2 + 2\Delta E_{c\uparrow\downarrow}^{\text{CDW}})} \quad (7)$$

and the corresponding  $\Delta E_{\text{tot}}$  is

$$\Delta E_{\text{tot, min}} = -\frac{(np\delta V_Q)^2 \cos^2(\phi_Q - \phi_0)}{16(\kappa^2 + 2\Delta E_{c\uparrow\downarrow}^{\text{CDW}})}. \quad (8)$$

It is now evident that the phase  $\phi_0$  of the SDW can shift to the value  $\phi_Q$  of the perturbation, so as to optimize the energy (8).

Thus the spin-split phase shift leads to an additional

$$\delta V(\mathbf{r}) = \delta V_q \{ \cos[(\mathbf{q} - \mathbf{Q}) \cdot \mathbf{r} + (\phi_q - \phi_0)] \cos(\mathbf{Q} \cdot \mathbf{r} + \phi_0) - \sin[(\mathbf{q} - \mathbf{Q}) \cdot \mathbf{r} + (\phi_q - \phi_0)] \sin(\mathbf{Q} \cdot \mathbf{r} + \phi_0) \}. \quad (11)$$

Because  $|\mathbf{q} - \mathbf{Q}|$  is small, the coefficient of the first term in Eq. (11) is slowly varying. Accordingly it induces a slowly varying spin-split phase

$$\delta\phi \cos[(\mathbf{q} - \mathbf{Q}) \cdot \mathbf{r} + (\phi_q - \phi_0)],$$

which we will call a (static) spin-split phason (SSPN). The response of the electron density to this SSPN is obtained by substituting this r-dependent phase modulation for the (constant)  $\delta\phi$  in Eq. (4),

$$\begin{aligned} \delta n(\mathbf{r}) &= -np \sin\{\delta\phi \cos[(\mathbf{q} - \mathbf{Q}) \cdot \mathbf{r} + (\phi_q - \phi_0)]\} \cos(\mathbf{Q} \cdot \mathbf{r} + \phi_0) \\ &\cong -\frac{np \delta\phi}{2} \{ \cos(\mathbf{q} \cdot \mathbf{r} + \phi_q) + \cos[(\mathbf{q} - 2\mathbf{Q}) \cdot \mathbf{r} + \phi_q - 2\phi_0] \}. \end{aligned} \quad (12)$$

Notice that  $\delta n(\mathbf{r})$  has split into two parts, one with wave vector  $\mathbf{q}$ , and the other with wave vector  $\mathbf{q} - 2\mathbf{Q}$ . The second term in Eq. (11) induces a (static) spin-split amplitude modulation which also causes a density response, since it is in phase with the second term (the  $\sigma_z$ -dependent one) of Eq. (2). For simplicity we shall neglect this effect because amplitude modulation is generally inhibited (energetically) relative to phase modulation.

The Coulomb energy associated with  $\delta n(\mathbf{r})$ , Eq. (12), now has two terms:

$$\Delta E_s = \frac{\pi e^2 n^2 p^2 (\delta\phi)^2}{4} \left[ \frac{1}{q^2} + \frac{1}{(\mathbf{q} - 2\mathbf{Q})^2} \right]. \quad (13)$$

This expression can be expanded to second order in the small quantity,  $\mathbf{q} - \mathbf{Q}$ . We find

$$\Delta E_s \cong (\frac{1}{2}\kappa^2 + C_{\alpha\beta} W_+^\alpha W_+^\beta) (\delta\phi)^2, \quad (14)$$

where  $\kappa$  is the same as in Eq. (6),  $\mathbf{W}_+ = \mathbf{q} - \mathbf{Q}$ , and  $C_{\alpha\beta} = \kappa^2(4Q_\alpha Q_\beta / Q^2 - \delta_{\alpha\beta}) / Q^4$ .  $\alpha$  and  $\beta$  denote the axes in an arbitrary Cartesian coordinate system.  $\delta_{\alpha\beta}$  is a Kronecker  $\delta$  function (and we have employed a summation convention over repeated indices).

One should expect that the energy of an SSPN differs slightly from that of a normal phason having the same amplitude and wave vector. The only differences come

charge response (over and above the usual Lindhard response):

$$-e\delta n(\mathbf{r}) = \frac{en^2 p^2 \delta V_Q}{4(\kappa^2 + 2\Delta E_{c\uparrow\downarrow}^{\text{CDW}})} \cos(\mathbf{Q} \cdot \mathbf{r} + \phi_Q). \quad (9)$$

It is important to appreciate that this additional response applies only for a perturbation having wave vector  $\mathbf{Q}$ . We will now show that the magnitude of Eq. (9) is the maximum value of a peak in three-dimensional  $\mathbf{q}$  space; i.e., the magnitude falls off as  $\mathbf{q}$  deviates from  $\mathbf{Q}$  in all directions.

Consider a perturbing potential having wave vector  $\mathbf{q}$  very close to  $\mathbf{Q}$ :

$$\delta V(\mathbf{r}) = \delta V_q \cos(\mathbf{q} \cdot \mathbf{r} + \phi_q). \quad (10)$$

This potential can be decomposed into two parts, one in phase with the spin-independent part of Eq. (2), and the other out of phase:

from  $\Delta E_s$ , in Eq. (14), and the  $\mathbf{q}$ -independent part of the electronic correlation energy, which can be derived from Eq. (A13) of Ref. 21. This latter contribution is,

$$\Delta E_c = -\Delta E_{c\uparrow\downarrow}^{\text{CDW}} [J_0(2\delta\phi) - 1], \quad (15)$$

where  $J_0(x)$  is the zeroth-order Bessel function. It is easy to show that the energy  $\Delta E_{np}$  of a (static) normal phason with wave vector  $\mathbf{W}_+$  is proportional to  $W_+^\alpha W_+^\beta (\delta\phi)^2$ .<sup>24</sup> Thus, to second order in  $\delta\phi$ , the electronic energy increment caused by the induced SSPN can be written as

$$\begin{aligned} \Delta E_{\text{ssp}} &\cong \Delta E_s + \Delta E_c + \Delta E_{np} \\ &\cong \frac{1}{2}\kappa^2 (\delta\phi)^2 + \Delta E_{c\uparrow\downarrow}^{\text{CDW}} (\delta\phi)^2 \\ &\quad + B_{\alpha\beta} W_+^\alpha W_+^\beta (\delta\phi)^2. \end{aligned} \quad (16)$$

All of the  $\mathbf{q}$ -dependent terms in  $\Delta E_{np}$  and  $\Delta E_s$  have been included in the last term of Eq. (16).  $B_{\alpha\beta}$ , which is expected to be a positive definite, second-order tensor, depends on the band structure and on the Fermi surface of the metal, as well as the on amplitude of the SDW.

The total-energy change, Eq. (5), becomes in this case [on using Eq. (16)]

$$\begin{aligned} \Delta E_{\text{tot}} &\cong -\frac{1}{4}np \delta V_q \delta\phi + \frac{1}{2}\kappa^2 (\delta\phi)^2 \\ &\quad + \Delta E_{c\uparrow\downarrow}^{\text{CDW}} (\delta\phi)^2 + B_{\alpha\beta} W_+^\alpha W_+^\beta (\delta\phi)^2. \end{aligned} \quad (17)$$

The additional factor  $\frac{1}{2}$  in the first three terms [when compared to Eqs. (5) and (6)] can be attributed to the fact that the density response has split into two Fourier components, as found in Eq. (12). From Eq. (17) we can obtain the equilibrium value for  $\delta\phi$ :

$$\delta\phi = \frac{np \delta V_{\mathbf{q}}}{4(\kappa^2 + 2 \Delta E_{c\uparrow\downarrow}^{\text{CDW}} + 2B_{\alpha\beta} W_+^\alpha W_+^\beta)}. \quad (18)$$

We are now ready to find the charge susceptibility at-

tributable to the SSPN mechanism. From Eqs. (10) and (12), it is easy to see that a complex external perturbation,

$$\begin{aligned} \delta V(\mathbf{r}) &= \delta V_{\mathbf{q}} e^{i\phi_{\mathbf{q}}} e^{i\mathbf{q}\cdot\mathbf{r}} \\ &= \delta V_{\mathbf{q}} \cos(\mathbf{q}\cdot\mathbf{r} + \phi_{\mathbf{q}}) \\ &\quad + i \delta V_{\mathbf{q}} \cos\left[\mathbf{q}\cdot\mathbf{r} + \phi_{\mathbf{q}} - \frac{\pi}{2}\right], \end{aligned} \quad (19)$$

induces a charge response,

$$\begin{aligned} -e[\delta n(\mathbf{r})] &\cong \frac{1}{2}enp \delta\phi \{\cos(\mathbf{q}\cdot\mathbf{r} + \phi_{\mathbf{q}}) + \cos[(\mathbf{q}-2\mathbf{Q})\cdot\mathbf{r} + \phi_{\mathbf{q}} - 2\phi_0]\} \\ &\quad + \frac{1}{2}ienp \delta\phi \{\cos(\mathbf{q}\cdot\mathbf{r} + \phi_{\mathbf{q}} - \frac{1}{2}\pi) + \cos[(\mathbf{q}-2\mathbf{Q})\cdot\mathbf{r} + \phi_{\mathbf{q}} - \frac{1}{2}\pi - 2\phi_0]\} \\ &= \frac{1}{2}enp \delta\phi e^{i\phi_{\mathbf{q}}} e^{i\mathbf{q}\cdot\mathbf{r}} + \frac{1}{2}enp \delta\phi e^{i\phi_{\mathbf{q}}} e^{i[(\mathbf{q}-2\mathbf{Q})\cdot\mathbf{r} - 2\phi_0]} \\ &\cong \chi^{\text{ssp}}(\mathbf{q}, \mathbf{q}) \delta V_{\mathbf{q}} e^{i\phi_{\mathbf{q}}} e^{i\mathbf{q}\cdot\mathbf{r}} + \chi^{\text{ssp}}(\mathbf{q}-2\mathbf{Q}, \mathbf{q}) \delta V_{\mathbf{q}} e^{i\phi_{\mathbf{q}}} e^{i[(\mathbf{q}-2\mathbf{Q})\cdot\mathbf{r}]}, \end{aligned} \quad (20)$$

where  $\delta\phi$  is given by Eq. (18). It must be noted that the SSPN mechanism leads to a charge susceptibility having both a diagonal term  $\chi^{\text{ssp}}(\mathbf{q}, \mathbf{q})$  and an off-diagonal term  $\chi^{\text{ssp}}(\mathbf{q}-2\mathbf{Q}, \mathbf{q})$ . Both terms have the same magnitude:

$$\chi^{\text{ssp}}(\mathbf{q}', \mathbf{q}) = \begin{cases} \frac{en^2 p^2}{8(\kappa^2 + 2 \Delta E_{c\uparrow\downarrow}^{\text{CDW}} + 2B_{\alpha\beta} W_+^\alpha W_+^\beta)}, & \mathbf{q}' = \mathbf{q} \\ \frac{en^2 p^2 e^{-2i\phi_0}}{8(\kappa^2 + 2 \Delta E_{c\uparrow\downarrow}^{\text{CDW}} + 2B_{\alpha\beta} W_+^\alpha W_+^\beta)}, & \mathbf{q}' = \mathbf{q} - 2\mathbf{Q} \\ 0, & \text{otherwise.} \end{cases} \quad (21a)$$

$$\chi^{\text{ssp}}(\mathbf{q}', \mathbf{q}) = \begin{cases} \frac{en^2 p^2 e^{-2i\phi_0}}{8(\kappa^2 + 2 \Delta E_{c\uparrow\downarrow}^{\text{CDW}} + 2B_{\alpha\beta} W_+^\alpha W_+^\beta)}, & \mathbf{q}' = \mathbf{q} - 2\mathbf{Q} \\ 0, & \text{otherwise.} \end{cases} \quad (21b)$$

$$0, \text{ otherwise.} \quad (21c)$$

Recall, of course, that these expressions are valid only for  $\mathbf{q}$  close to  $\mathbf{Q}$ . These extra charge responses (over and above the usual Lindhard response) decrease rapidly as  $\mathbf{q}$  moves away from the wave vector  $\mathbf{Q}$  of the SDW, as defined following Eq. (14), i.e.,  $\mathbf{W}_+ = \mathbf{q} - \mathbf{Q}$ .

There is a general symmetry property for a charge susceptibility

$$\chi(\mathbf{q}', \mathbf{q}) = \chi^*(-\mathbf{q}', -\mathbf{q}), \quad (22)$$

where  $\chi^*$  is the complex conjugate of  $\chi$ . So for  $\mathbf{q}$  close to  $-\mathbf{Q}$ ,

$$\chi^{\text{ssp}}(\mathbf{q}', \mathbf{q}) = \begin{cases} \frac{en^2 p^2}{8(\kappa^2 + 2 \Delta E_{c\uparrow\downarrow}^{\text{CDW}} + 2B_{\alpha\beta} W_-^\alpha W_-^\beta)}, & \mathbf{q}' = \mathbf{q} \\ \frac{en^2 p^2 e^{2i\phi}}{8(\kappa^2 + 2 \Delta E_{c\uparrow\downarrow}^{\text{CDW}} + 2B_{\alpha\beta} W_-^\alpha W_-^\beta)}, & \mathbf{q}' = \mathbf{q} + 2\mathbf{Q} \\ 0, & \text{otherwise,} \end{cases} \quad (23a)$$

$$\chi^{\text{ssp}}(\mathbf{q}', \mathbf{q}) = \begin{cases} \frac{en^2 p^2 e^{2i\phi}}{8(\kappa^2 + 2 \Delta E_{c\uparrow\downarrow}^{\text{CDW}} + 2B_{\alpha\beta} W_-^\alpha W_-^\beta)}, & \mathbf{q}' = \mathbf{q} + 2\mathbf{Q} \\ 0, & \text{otherwise,} \end{cases} \quad (23b)$$

$$0, \text{ otherwise,} \quad (23c)$$

with  $\mathbf{W}_- = \mathbf{q} + \mathbf{Q}$ .

A schematic plot of the *diagonal* charge susceptibility of a SDW state is presented in Fig. 2 and is essentially the Lindhard response plus the additional contributions from Eqs. (21) and (23). The most important features appearing in Fig. 2 are the three-dimensional anisotropic peaks located at  $\pm\mathbf{Q}$  in  $\mathbf{q}$  space. As we will show in Sec. V, these peaks will provide an explanation of the frequency dips in the phonon spectrum of Pb near the  $\{100\}$  zone-boundary points.

### III. CORE-SHELL EXCHANGE ENERGY

The dynamic pseudopotential theory of phonons proposed by WO has been successful in reproducing phonon dispersion curves for more than a dozen cubic metals.<sup>15,25</sup> One key point of the theory is the division of each ion into an inner core and a last-filled electron shell, so that the shell may be allowed to vibrate relative to the core. The only interaction, considered by WO, between the shell and the core was the Coulomb interaction, screened

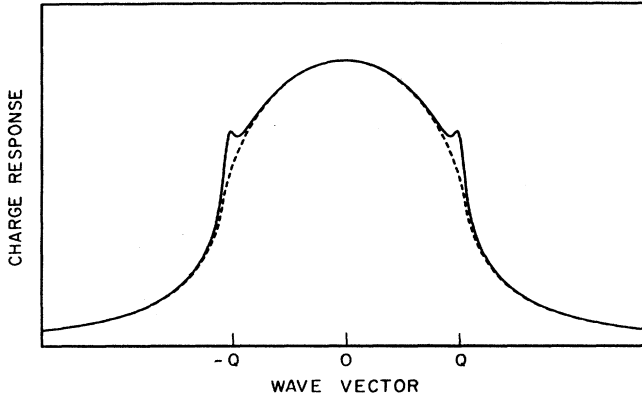


FIG. 2. Charge susceptibility of an electron gas vs  $q$  in a direction  $\hat{l}$ , parallel to  $Q$  of the SDW. The peaks at  $\pm Q$  arise from the static spin-split phase (SSPN) mechanism. The dashed line is the Lindhard response (when there is no SDW). The SSPN peaks are sharp in all three ( $q$  space) directions, near  $q = \pm Q$ .

(of course) by the conduction electrons. In heavy metals (such as Pb) allowance for the shell vibration causes a reduction in the zone-boundary frequencies by as much as 60%, compared to a rigid-ion model. It is to be expected that for a real ion, besides the Coulomb interaction, there is also a significant exchange interaction between electrons of the core and those of the shell (because their wave functions overlap). Naturally core-shell exchange should be included in the lattice dynamics of heavy metals. The core-shell exchange energy will depend on the electron-density distributions in both the core and the shell, and the overlap will change when the shell moves relative to the core. It can be shown that the core-shell exchange energy for a single ion has the following form:

$$u_{\text{ex}} = u_{\text{ex},0} + \mu \frac{ne^2}{(2\pi)^2} |\mathbf{u} - \mathbf{v}|^2, \quad (24)$$

where  $u_{\text{ex},0}$  is the value of  $u_{\text{ex}}$  for a rigid ion.  $\mathbf{u}$  and  $\mathbf{v}$  are the displacements of the core and shell, relative to the lattice site.  $\mu$  is a core-shell exchange energy parameter which, together with the other parameters in WO, can be used to fit the phonon dispersion curves. The factor involving  $ne^2$ , in the second term of Eq. (24), was introduced so that  $\mu$  would be a dimensionless quantity. The sign of  $\mu$  could be either positive or negative, depending on the electron-density distributions of the core and shell.

The change in core-shell exchange energy (per unit volume) arising from the core displacements,

$$\mathbf{u}(\mathbf{L}) = A_c \hat{\alpha}_q \cos(\mathbf{q} \cdot \mathbf{L}), \quad (25)$$

and the shell displacements,

$$\mathbf{v}(\mathbf{L}) = A_s \hat{\beta}_q \cos(\mathbf{q} \cdot \mathbf{L}), \quad (26)$$

can be easily found by summing over lattice sites  $\{\mathbf{L}\}$ ,

$$\Delta U_{\text{ex}} = \mu \pi n^2 e^2 |A_c \hat{\alpha}_q - A_s \hat{\beta}_q|^2, \quad (27)$$

where  $\hat{\alpha}_q$  and  $\hat{\beta}_q$  are unit polarization vectors of the core

and shell displacements.  $\Delta U_{\text{ex}}$  will be an additional potential energy term in the lattice-dynamics formulation.

It is interesting to note from Eq. (24) that a positive  $\mu$  for the core-shell exchange interaction is equivalent to putting a spring between the core and the shell, as first suggested by Dick and Overhauser.<sup>26</sup> Obviously,  $\mu = 0$  corresponds to the normal deformable shell model discussed by WO. A positive  $\mu$  makes it harder for a shell to vibrate (relative to its core) and increases the zone-boundary frequencies. The limit of large  $\mu$  leads to recovery of the rigid-ion pseudopotential model. Therefore  $\mu$  is a measure of the rigidity of the ions and allows the dynamic pseudopotential model to range between the deformable-ion model and the rigid-ion model.

#### IV. REVIEW OF LATTICE DYNAMICS

In Sec. II we found that the existence of a SDW state introduces two extra charge-response components: one at  $\mathbf{q}$ , the applied periodicity, and the other at  $\mathbf{q} - 2\mathbf{Q}$ . When  $\mathbf{q}$  is near  $\mathbf{Q}$  both response components exhibit a peak. Whether or not such a peak leads to cusps in the phonon dispersion curves depends on the phonon polarizations and on the parameters describing the peak. It is straightforward to extend the WO theory to include both the effects of SDW's and of the core-shell exchange interaction discussed in the previous section. For the sake of simplicity, only the diagonal charge response will be taken into account. We have found that neglect of the off-diagonal response  $\epsilon(\mathbf{q} - 2\mathbf{Q}, \mathbf{q})$  does not alter significantly any features in our calculated phonon spectra. With the core and shell displacements given by Eqs. (25) and (26), the equations of motion are found to be

$$\begin{bmatrix} \underline{D}_p(cc) + \mu \underline{I} & \underline{D}_p(cs) - \mu \underline{I} \\ \underline{D}_p(sc) - \mu \underline{I} & \underline{D}_p(ss) + \mu \underline{I} \end{bmatrix} \begin{bmatrix} A_c \hat{\alpha}_q \\ A_s \hat{\beta}_q \end{bmatrix} = \begin{bmatrix} \frac{M}{4\pi n} \omega^2 A_c \hat{\alpha}_q \\ \frac{zm}{4\pi n} \omega^2 A_s \hat{\beta}_q \end{bmatrix}, \quad (28)$$

where a monoatomic Bravais lattice has been assumed.  $n$  is the density of atoms, and  $z$  is the number of electrons in each last-filled shell.  $M$  and  $m$  are the ion and electron masses.  $\underline{I}$  is the  $3 \times 3$  unit matrix, and the  $3 \times 3$   $\underline{D}_p$ 's are given by

$$\begin{aligned} [\underline{D}_p(cc)]_{ij} &= \sum_{\mathbf{G}} \frac{\bar{\rho}_c(\mathbf{G} + \mathbf{q}) \bar{\rho}_c(\mathbf{G} + \mathbf{q})}{|\mathbf{G} + \mathbf{q}|^2 \epsilon_{cc}(\mathbf{G} + \mathbf{q})} (\mathbf{G} + \mathbf{q})_i (\mathbf{G} + \mathbf{q})_j \\ &\quad - \sum_{\mathbf{G}} \left[ \frac{\bar{\rho}_c(\mathbf{G}) \bar{\rho}_c(\mathbf{G})}{|\mathbf{G}|^2 \epsilon_{cc}(\mathbf{G})} (\mathbf{G})_i (\mathbf{G})_j \right. \\ &\quad \left. + \frac{\bar{\rho}_c(\mathbf{G}) \bar{\rho}_s(\mathbf{G})}{|\mathbf{G}|^2 \epsilon_{cs}(\mathbf{G})} (\mathbf{G})_i (\mathbf{G})_j \right], \quad (29) \end{aligned}$$

and

$$\begin{aligned} [\underline{D}_p(cs)]_{ij} &= \sum_{\mathbf{G}} \frac{\bar{\rho}_c(\mathbf{G} + \mathbf{q}) \bar{\rho}_s(\mathbf{G} + \mathbf{q})}{|\mathbf{G} + \mathbf{q}|^2 \epsilon_{cs}(\mathbf{G} + \mathbf{q})} \\ &\quad \times (\mathbf{G} + \mathbf{q})_i (\mathbf{G} + \mathbf{q})_j. \quad (30) \end{aligned}$$

$\underline{D}_p(sc)$  is the transpose of  $\underline{D}_p(cs)$ , and  $\underline{D}_p(ss)$  can be obtained from Eq. (29) by interchange of  $c$  and  $s$ . In Eqs. (29) and (30),  $\{\mathbf{G}\}$  and  $\{\mathbf{G}'\}$  are reciprocal lattice vectors, and the prime on the second sum in Eq. (29) indicates omission of the term with  $\mathbf{G}'=0$ .  $\bar{\rho}_c(\mathbf{Q})$  and  $\bar{\rho}_s(\mathbf{Q})$  are Fourier transforms of the core and shell pseudocharge densities. For Pb, the last-filled shell is  $5d$ , hence  $\bar{\rho}_c(\mathbf{Q})$  and  $\bar{\rho}_s(\mathbf{Q})$  are, according to WO,

$$\bar{\rho}_c(\mathbf{Q}) = 14e \exp(-\frac{1}{2}R_c^2 Q^2), \quad (31)$$

and

$$\bar{\rho}_s(\mathbf{Q}) = -10e(1 - \frac{2}{3}R_s^2 Q^2 + \frac{1}{15}R_s^4 Q^4) \exp(-\frac{1}{2}R_s^2 Q^2), \quad (32)$$

where  $e$  is the electron charge.  $R_c$  and  $R_s$  are radius parameters for the core and shell and are adjusted to fit the dispersion curves.

The core-core dielectric function  $\epsilon_{cc}(\mathbf{q})$ , the core-shell dielectric function  $\epsilon_{cs}(\mathbf{q})$ , and the shell-shell dielectric function  $\epsilon_{ss}(\mathbf{q})$  are given by the same expressions as in WO, except that the usual Lindhard response function  $Q_0(\mathbf{q})$  is replaced by  $Q_0(\mathbf{q}) + Q'_T(\mathbf{q})$ , where  $Q'_T(\mathbf{q})$  is the extra (diagonal) response caused by the SDW's, defined below in Eqs. (38) and (39),

$$\epsilon_{cc}^{-1}(\mathbf{q}) = 1 - \frac{Q_0(\mathbf{q}) + Q'_T(\mathbf{q})}{1 + (1 - G_+) [Q_0(\mathbf{q}) + Q'_T(\mathbf{q})]}, \quad (33)$$

$$\epsilon_{cs}^{-1}(\mathbf{q}) = 1 - \frac{(1 - \gamma_s G_+) [Q_0(\mathbf{q}) + Q'_T(\mathbf{q})]}{1 + (1 - G_+) [Q_0(\mathbf{q}) + Q'_T(\mathbf{q})]}, \quad (34)$$

and

$$\epsilon_{ss}^{-1} = 1 - \frac{(1 - \gamma_s G_+)^2 [Q_0(\mathbf{q}) + Q'_T(\mathbf{q})]}{1 + (1 - G_+) [Q_0(\mathbf{q}) + Q'_T(\mathbf{q})]}. \quad (35)$$

$\gamma_s$  is the parameter characterizing the exchange interaction between shell electrons and the conduction-electron sea, and  $G_+(q)$  is the spin-symmetric exchange-correlation local-field function.<sup>27</sup> We use the form suggested by Hubbard,<sup>28</sup>

$$G_+(x) = \frac{1.1x^2}{1 + 1.7x^2}, \quad (36)$$

but with coefficients which lead to the correct limiting behavior near  $x=0$  and  $x=\infty$ . ( $x=q/2k_F$ , and  $k_F$  is the Fermi radius.) The usual Lindhard density response function is given by

$$Q_0(\mathbf{q}) = \frac{m_b e^2}{\pi \hbar^2 k_F x^2} \left[ \frac{1}{2} + \frac{1-x^2}{8x} \ln \left[ \frac{(1-x)^2 + \delta}{(1-x)^2 + \delta} \right] \right]. \quad (37)$$

For Pb the band mass  $m_b$  is 0.77 times the free-electron mass.<sup>15</sup> A small quantity  $\delta$  has been introduced to prevent the singularity in the logarithmic term from creating artifacts in the computer calculations. We set  $\delta=0.001$  as in WO.

The physical properties of Pb, and especially its pho-

non spectrum, show no indication that the symmetry is less than cubic. The broken symmetry which would result, for example, from a single SDW would contradict the data at the outset. Accordingly we shall use a multiple-Q SDW state, for which there is a full cubic family, having wave vectors  $\{\mathbf{Q}_i\}$ , such that any rotation of cubic symmetry reproduces  $\{\mathbf{Q}_i\}$ . The charge response derived in Sec. II must be amended to include contributions from all SDW's. The total response is then

$$Q'_T(\mathbf{q}) = \sum_i [Q_{i+}^{\text{ssp}}(\mathbf{q}) + Q_{i-}^{\text{ssp}}(\mathbf{q})], \quad (38)$$

with

$$Q_{i\pm}^{\text{ssp}}(\mathbf{q}) \equiv \frac{4\pi e}{q^2} \chi_{i\pm}^{\text{ssp}}(\mathbf{q}). \quad (39)$$

$\chi_{i\pm}^{\text{ssp}}(\mathbf{q})$  is the diagonal response (for  $\mathbf{q}$  close to  $\pm\mathbf{Q}_i$ ) of the  $i$ th SDW component having wave vector  $\mathbf{Q}_i$ . The number of components depends on the direction of  $\mathbf{Q}$ : For  $\mathbf{Q}=(2\pi/a)(2,1,0)$  or  $(2\pi/a)(2,1,1)$  there are 12 equivalent axes; for  $\mathbf{Q}=(2\pi/a)(1,1,0)$  there are 6; and for  $\mathbf{Q}=(2\pi/a)(1,0,0)$ , there are 3.

The most important feature of  $\chi_{i\pm}^{\text{ssp}}(\mathbf{q})$  is that near  $\mathbf{q}=\pm\mathbf{Q}_i$  it has sharp peaks, which will (as we shall show) explain the unexpected dips in the phonon dispersion curves of Pb. Although the peaks in  $\chi^{\text{ssp}}$ , derived in Eqs. (21) and (23), have a Lorentzian shape, it must be remembered that the derivation was based on the smallness of  $|\mathbf{q}-\mathbf{Q}|$ . Consequently the Lorentzian tails for large  $|\mathbf{q}-\mathbf{Q}|$  are not of physical significance. There is a practical advantage in not having such tails when summing over thousands of reciprocal lattice vectors. So we replace the Lorentzian forms with Gaussian ones:

$$Q_{i\pm}^{\text{ssp}}(\mathbf{q}) = \frac{A}{x^2} \exp(-\Pi_{i\pm}), \quad (40)$$

and

$$\Pi_{i\pm} = B_{\alpha\beta} W_{i\pm}^\alpha W_{i\pm}^\beta, \quad (41)$$

where  $\mathbf{W}_{i\pm} = \mathbf{q} \mp \mathbf{Q}_i$ ,  $x = q/2k_F$ , and  $B_{\alpha\beta}$  is a positive-definite second-order tensor, i.e., Eq. (41) represents an ellipsoid centered at  $\pm\mathbf{Q}_i$  in reciprocal space. If  $\hat{\mathbf{t}}$ ,  $\hat{\mathbf{l}}$ , and  $\hat{\mathbf{v}}$  are unit vectors along the three principal axes, Eq. (41) becomes

$$\Pi_{i\pm} = B_t^2 W_{i\pm}^t{}^2 + B_l^2 W_{i\pm}^l{}^2 + B_v^2 W_{i\pm}^v{}^2 \quad (42)$$

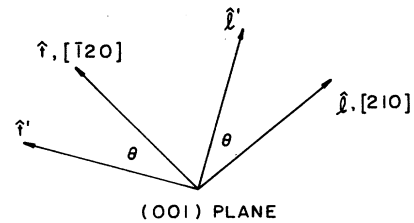


FIG. 3. Principal axes  $\hat{\mathbf{t}}$ ,  $\hat{\mathbf{l}}$ , and  $\hat{\mathbf{v}}$  of an SSPN ellipsoid for a SDW with  $\mathbf{Q}=(2\pi/a)(2,1,0)$ .  $\hat{\mathbf{v}}$ , not shown, is perpendicular to the paper [i.e., an (001) plane].  $\hat{\mathbf{l}}$  is parallel to  $\mathbf{Q}$ .  $\hat{\mathbf{t}}$  and  $\hat{\mathbf{l}}$ , obtained by rotating the ellipsoid about the  $\hat{\mathbf{v}}$  axis by  $\theta$ , together with  $\hat{\mathbf{v}}$  is an alternative set of principal axes.

in the  $\hat{t}, \hat{l}, \hat{v}$  coordinate system.  $B_t, B_l,$  and  $B_v$  are the inverse widths of the peaks along each principal axis. The coefficient  $A$  in Eq. (40) and the  $B$ 's in Eq. (42) are determined by fitting the observed cusps near  $\{100\}$  points in the phonon spectrum.

## V. RESULTS AND DISCUSSION

In the following, we will show that the existence of commensurate SDW's with  $\{Q_i\}$  along special symmetry directions gives a unique explanation to the frequency cusps that appear in Pb's phonon dispersion curves. As mentioned before, we omit the off-diagonal charge response of the SDW's, i.e., the terms with  $q' = q \pm 2Q_i$  in Eqs. (21) and (23). We have found that inclusion of such off-diagonal terms merely forces us to readjust  $A$  and the  $B$ 's in Eqs. (40) and (42) and does not have a significant effect on the phonon dispersion curves. The downward cusps in both longitudinal and transverse modes are centered at the  $\{100\}$  points of the Brillouin zone. We have found the SDW families must involve  $\{Q_i\}$  located at superstructure points in order to reproduce this feature. The SDW families we have investigated are the following ones.

### A. $\{210\}$ SDW family

For this case we assume that Pb has twelve SDW's, each one with a  $Q$  equal to one of the twelve  $\{210\}$  superlattice vectors. Consider the SDW with  $Q = (2\pi/a)(2, 1, 0)$ . The directions of some related vectors in reciprocal space are shown in Fig. 3, in which we have set the principal axis  $\hat{v}$ , defined in Eq. (42), parallel to the  $[001]$  direction (because such a choice is required by symmetry).  $\hat{t}$  is the unit vector parallel to  $Q$ , and  $\hat{l} = \hat{v} \times \hat{t}$  is the third principal axis. However, symmetry does not require that  $\hat{l}$  be parallel to  $Q$ , so we have entertained all alternatives, i.e.,  $\hat{l}$  and  $\hat{l}'$  (both perpendicular to  $\hat{v}$ ) rotated by an angle  $\theta$  about the  $\hat{v}$  axis. The SSPN function  $\Pi_+$ , given in Eq. (42), but expressed in the  $\hat{t}, \hat{l}, \hat{v}$

coordinate system is, for this alternative,

$$\begin{aligned} \Pi_+ = & (B_t^2 \cos^2 \theta + B_l^2 \sin^2 \theta) (W_+^t)^2 \\ & + (B_t^2 \sin^2 \theta + B_l^2 \cos^2 \theta) (W_+^l)^2 \\ & + (B_t^2 - B_l^2) \sin(2\theta) W_+^t W_+^l + B_v^2 (W_+^v)^2. \end{aligned} \quad (43)$$

We studied the lattice dynamics for several values of  $\theta$  (from 0 to  $\pi$ ) and became convinced that  $\theta=0$  was the best. Therefore we fixed  $\hat{t}, \hat{l},$  and  $\hat{v}$  as the three principal axes of the SSPN ellipsoid located at  $Q$ . Obviously, cubic rotations generate the principal axes appropriate to the 23 remaining ellipsoids.

It should be emphasized that the present work cannot be expected to fit all details of the phonon dispersion in Pb because we have not included effects that could arise from the (relatively small) anisotropy of the Fermi surface.<sup>18,29</sup> Figure 4 shows the experimental data and the calculated dispersion curves resulting from a  $\{210\}$  SDW family (solid lines). The dashed lines are the computed spectra with  $A=0$ , i.e., no SDW's. The cusps created by the SDW's are satisfactory, and the overall agreement with the experimental data is very good.

The discrepancy in the  $[\xi\xi\xi]L$  branch near the zone boundary is usually attributed to an enhanced Kohn anomaly.<sup>17</sup> Experimental data from Pb-Tl alloys<sup>30,31</sup> reveal that the location of the Kohn anomaly moves away from the zone boundary and that the longitudinal phonon frequencies near the  $(0.5, 0.5, 0.5)$  point increase rapidly. Therefore, if there were no enhanced Kohn anomaly, the calculated frequencies would likely be quite close to the experimental ones.

Since the value of  $A$  needed to fit the data is quite small, the particular shape (Gaussian, Lorentzian, etc.) if the SSPN charge response  $\chi_{i\pm}^{\text{SSPN}}(\mathbf{q})$  is not important. To demonstrate this point we show in Fig. 5 the calculated phonon spectrum based on Lorentzian peaks,

$$Q_{i\pm}^{\text{SSPN}}(\mathbf{q}) = \frac{A}{x^2(1 + \Pi_{i\pm})}, \quad (44)$$

$\Pi_{i\pm}$  is still given by Eq. (42). Of course, the parameters

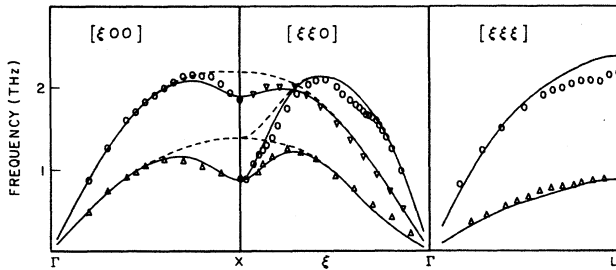


FIG. 4. Theoretical phonon spectrum of Pb with a cubic family of (twelve)  $\{210\}$  SDW's. The data points were taken from Brockhouse *et al.*, Ref. 17, for  $T=100$  K. The parameters used in computing the solid curves are  $R_s = 1.273/(2k_F)$ ,  $R_c = 2.04/(2k_F)$ ,  $\gamma_s = 0.08$ ,  $\mu = 0$ ,  $A = 0.026$ ,  $B_t = 8/(2k_F)$ ,  $B_l = 15/(2k_F)$ , and  $B_v = 2.8/(2k_F)$ . The SSPN charge response used for the solid curves was the Gaussian type, Eq. (40). The dashed curves were computed with  $A=0$ , i.e., no SDW;  $R_s, R_c,$  and  $\gamma_s$  were unchanged.

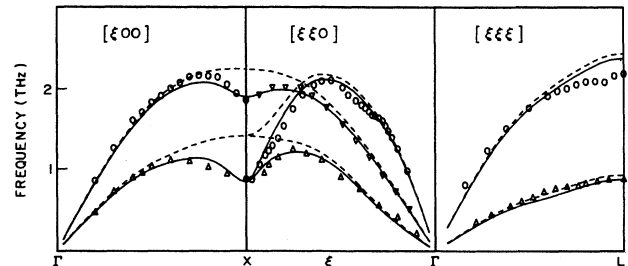


FIG. 5. Theoretical phonon spectrum of Pb with a cubic family of (twelve)  $\{210\}$  SDW's. The data points were taken from Brockhouse *et al.*, Ref. 17, for  $T=100$  K. The parameters used in computing the solid curves are  $R_s = 1.273/(2k_F)$ ,  $R_c = 2.0/(2k_F)$ ,  $\gamma_s = 0.07$ ,  $\mu = 0$ ,  $A = 0.02$ ,  $B_t = 10/(2k_F)$ ,  $B_l = 25/(2k_F)$ , and  $B_v = 3.2/(2k_F)$ . The SSPN charge response used for the solid curves was the Lorentzian type, Eq. (44). The dashed curves were computed with  $A=0$ , i.e., no SDW;  $R_s, R_c,$  and  $\gamma_s$  were unchanged.

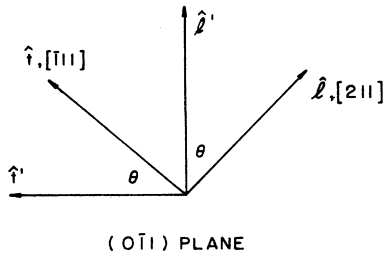


FIG. 6. Principal axes  $\hat{t}$ ,  $\hat{l}$ , and  $\hat{v}$  of an SSPN ellipsoid for a SDW with  $\mathbf{Q}=2\pi(2,1,1)/a$ .  $\hat{v}$ , not shown, is perpendicular to the paper [i.e., an  $(0\bar{1}1)$  plane].  $\hat{l}$  is parallel to  $\mathbf{Q}$ ,  $\hat{t}$ , and  $\hat{P}$ , obtained by rotating the ellipsoid about the  $\hat{v}$  axis by  $\theta$ , together with  $\hat{v}$  is an alternative set of principal axes.

$R_c$ ,  $\gamma_s$ ,  $A$ , and  $B$  have been readjusted. Comparison of Fig. 5 with Fig. 4 shows that the fits are comparable.

### B. $\{211\}$ SDW family

For a SDW with  $\mathbf{Q}=(2\pi/a)(2,1,1)$ , the crystal symmetry allows us to choose the principal axis  $\hat{v}$ , defined in Eq. (42), along the  $\{0\bar{1}1\}$  direction. Some related vectors are shown in Fig. 6. By the same trials described above, we found that the best choice for  $\hat{l}$  is parallel to  $\mathbf{Q}$ . The remaining principal axis is, of course,  $\hat{t}=\hat{v}\times\hat{l}$ . Figure 7 compares the best fit obtained using  $\{211\}$  SDW's with the experimental data. In this case a positive core-shell exchange parameter  $\mu$  was optimum. The two cusps near the  $\{100\}$  zone-boundary points are again reproduced. However the agreement is not quite as good as that found using the  $\{210\}$  SDW family. With  $\{211\}$  SDW's the size of the dip for the transverse branch is generally two to three times smaller than the one for the longitudinal branch.

The appearance of the downward cusps in the calculated curves of Fig. 7 does not depend on using a nonzero  $\mu$ . The dotted curves were obtained upon setting  $\mu=0$  and

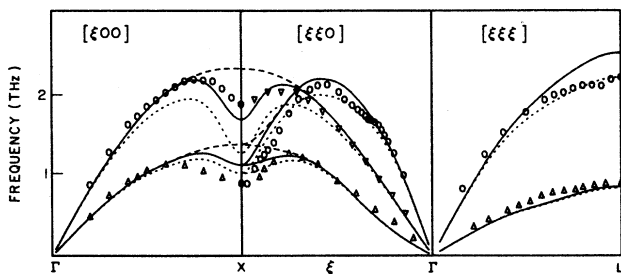


FIG. 7. Theoretical phonon spectrum of Pb with a cubic family of (twelve)  $\{211\}$  SDW's. The data points were taken from Brockhouse *et al.*, Ref. 17, for  $T=100$  K. The parameters used in computing the solid curves are  $R_s=1.273/(2k_F)$ ,  $R_c=2.04/(2k_F)$ ,  $\gamma_s=0.115$ ,  $\mu=35$ ,  $A=0.045$ ,  $B_l=10/(2k_F)$ ,  $B_t=15/(2k_F)$ , and  $B_v=6.5/(2k_F)$ . The SSPN charge response used for the solid curves was the Gaussian type, Eq. (40). The dotted curves were computed with  $\mu=0$ . The dashed curves were computed with  $A=0$ , i.e., no SDW;  $R_s$ ,  $R_c$ , and  $\gamma_s$  were unchanged (and  $\mu=35$ ).

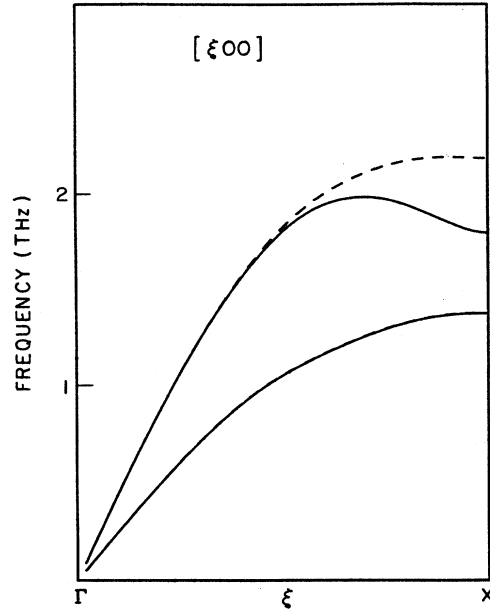


FIG. 8. Phonon spectrum of Pb along the  $[100]$  direction with a cubic family of (three)  $\{100\}$  SDW's. The parameters used are  $R_s=1.273/(2k_F)$ ,  $R_c=2.04/(2k_F)$ ,  $\gamma_s=0.08/(2k_F)$ ,  $\mu=0$ ,  $A=0.025$ ,  $B=8.6/(2k_F)$ . The SSPN charge response in Gaussian. The dashed curves were obtained upon setting  $A=0$ , i.e., no SDW. (Solid and dashed curves coincide for the transverse mode.)

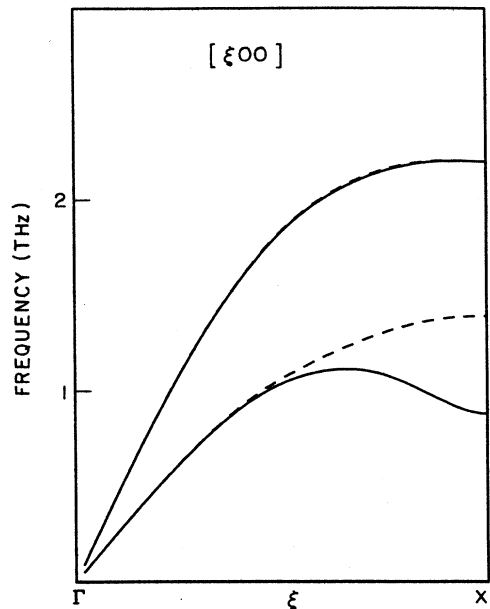


FIG. 9. Phonon spectrum of Pb along the  $[100]$  direction with a cubic family of (six)  $\{110\}$  SDW's. The parameters used were the same as in Fig. 8, except  $A=0.02$ . The dashed curves were obtained upon setting  $A=0$ , i.e., no SDW. (Solid and dashed curves coincide for the longitudinal mode.)

leaving all other parameters unchanged. In this case  $\mu$  has its largest effect on the longitudinal modes near the zone boundary.

### C. {100} and {110} SDW families

For either the {100} or the {110} SDW family, we find that only one of the cusps at the {100} zone-boundary points can be qualitatively reproduced. To illustrate this point schematically we choose all three  $B$ 's in Eq. (42) to equal the average of the three  $B$ 's found for the {210} SDW family. The calculated phonon spectra for the {100} family is shown in Fig. 8 and that for the {110} family is shown in Fig. 9. The {110} SDW family causes a large cusp in the transverse mode but has little effect on the longitudinal mode. The {100} SDW family reverses the result: A large cusp appears in the longitudinal branch, but the transverse branch remains unchanged. These observations can be understood easily by using the (simpler) rigid-ion model of lattice dynamics.<sup>22</sup> In this model there is no need to diagonalize a matrix, and the phonon frequencies along symmetry axes are given by

$$\omega^2(\mathbf{q}) = \frac{4\pi n}{M} \sum_{\mathbf{G}} \left[ \frac{\bar{\rho}^2(\mathbf{G}+\mathbf{q}) |(\mathbf{G}+\mathbf{q}) \cdot \hat{\alpha}_{\mathbf{q}}|^2}{|\mathbf{G}+\mathbf{q}|^2 \epsilon_{cc}(\mathbf{G}+\mathbf{q})} - \frac{\bar{\rho}^2(\mathbf{G}) |\mathbf{G} \cdot \hat{\alpha}_{\mathbf{q}}|^2}{|\mathbf{G}|^2 \epsilon_{cc}(\mathbf{G})} \right], \quad (45)$$

$\bar{\rho}(\mathbf{q}) = \bar{\rho}_c(\mathbf{q}) + \bar{\rho}_s(\mathbf{q})$  is the Fourier transform of the total-ion charge density, and  $\epsilon_{cc}(\mathbf{q})$  is the core-core dielectric function given by Eq. (33). For small SDW contributions  $Q'_T$  to the charge response,

$$\begin{aligned} \epsilon_{cc}^{-1}(\mathbf{q}) &\cong \left[ 1 - \frac{Q_0(\mathbf{q})}{1 + (1 - G_+) Q_0(\mathbf{q})} \right] \\ &\quad - \frac{Q'_T(\mathbf{q})}{[1 + (1 - G_+) Q_0(\mathbf{q})]^2} \\ &\cong \epsilon_{tt}^{-1}(\mathbf{q}) - \epsilon_{SDW}^{-1}(\mathbf{q}), \end{aligned} \quad (46)$$

where  $\epsilon_{tt}(\mathbf{q})$  is the ordinary test-charge—test-charge dielectric function, and  $\epsilon_{SDW}(\mathbf{q})$  is defined by

$$\epsilon_{SDW}^{-1}(\mathbf{q}) = \frac{Q'_T(\mathbf{q})}{[1 + (1 - G_+) Q_0(\mathbf{q})]^2}. \quad (47)$$

Since  $Q'_T(\mathbf{q})$  has a finite value only when  $\mathbf{q}$  is near  $\pm \mathbf{Q}$  for each of the SDW wave vectors,  $\epsilon_{SDW}^{-1}(\mathbf{G})$  is usually negligible. Therefore, upon substituting Eq. (46) into Eq. (45),  $\omega^2(\mathbf{q})$  is approximately

$$\omega^2(\mathbf{q}) \cong \omega_0^2(\mathbf{q}) - \frac{4\pi n}{M} \sum_{\mathbf{G}} \frac{\bar{\rho}^2(\mathbf{G}+\mathbf{q}) |(\mathbf{G}+\mathbf{q}) \cdot \hat{\alpha}_{\mathbf{q}}|^2}{|\mathbf{G}+\mathbf{q}|^2 \epsilon_{SDW}(\mathbf{G}+\mathbf{q})}. \quad (48)$$

$\omega_0(\mathbf{q})$  is the phonon frequency in the absence of SDW's.

Consider now the {100} SDW family, for which  $\epsilon_{SDW}^{-1}(\mathbf{G}+\mathbf{q})$  is negligible except when  $(\mathbf{G}+\mathbf{q})$  is near a {100} zone-boundary point. For  $\mathbf{q}=(1,0,0)$ , the only  $\mathbf{G}$ 's which satisfy this condition are  $\mathbf{G}=(0,0,0)$  or  $(-2,0,0)$ , for which  $(\mathbf{G}+\mathbf{q})=(\pm 1,0,0)$ . However,  $(\pm 1,0,0)$  is perpendicular to the polarization vector  $\hat{\alpha}_{\mathbf{q}}$  for transverse modes along [100]. So  $(\mathbf{G}+\mathbf{q}) \cdot \hat{\alpha}_{\mathbf{q}}=0$ ; and from Eq. (48), the {100} SDW family has little effect on the transverse branch along [100]. The absence of a cusp in the longitudinal branch with a {110} SDW family can be understood in the same way. We have also investigated the effects of a {300} SDW family, and found the same result as that for a {100} SDW family: Only a cusp in the longitudinal branch could be explained.

## VI. CONCLUSIONS

We have shown that a cubic family of small-amplitude SDW's, having  $\mathbf{Q}$ 's equal to {210} or {211} can explain the observed cusps in both longitudinal and transverse modes near the {100} zone-boundary points of Pb. The best fit was obtained using the {210} family, i.e., there are twelve SDW's, each having a wave vector  $\mathbf{Q}$  of the type  $\mathbf{Q}=(2\pi/a)(2,1,0)$ . ( $a$  is the lattice constant.)  $|\mathbf{Q}|=0.90(2k_F)$  for this case; and  $|\mathbf{Q}|=0.99(2k_F)$  for the {211} family. A definite choice between these two alternatives cannot be made at this time. The latter possibility satisfies the theoretical expectation,<sup>20</sup>  $|\mathbf{Q}| \cong 2k_F$ , but the former possibility allows the closest fit to the experimental phonon spectrum. (It is likely, of course, that band-structure effects might modify naive expectations about  $|\mathbf{Q}|$ .)

The temperature dependence of Pb's phonon spectrum has also been measured.<sup>32</sup> As is usually the case, the frequencies decrease (with increasing  $T$ ) almost everywhere in reciprocal space. However, near the {100} zone-boundary points they *increase*. It seems fair to say that the sizes of the (downward) cusps become smaller with increasing temperature. One way to interpret such behavior in terms of SDW theory is that thermally-induced phase modulation of the SDW's causes a reduction (and broadening) of the SSPN peaks in the charge response, which gives rise to the cusps.

It has been shown recently<sup>33</sup> that SDW's have profound effects on some superconducting properties. For example, the low-temperature tail in the electronic heat capacity of Pb,<sup>34</sup> which at 0.5 K is four orders of magnitude higher than it "ought" to be, can be explained with the SDW model envisioned in this paper. A fit to the heat-capacity data leads to an estimate for the SDW transition temperature at or above the melting point of Pb.<sup>33</sup> Anomalous behavior in ultrasonic attenuation at low temperatures and in the tunneling conductance of quench-condensed Pb NIS junctions can also be explained by the presence of SDW's.<sup>35</sup>

It goes without saying that the presence of SDW's in Pb would never be firmly established until magnetic scattering of neutrons is observed. Such experiments are feasible, though predictably difficult. The fractional modulation of each SDW is expected (from the heat-

capacity tail mentioned above) to be  $p \sim 1\%$ . Not only is this amplitude quite small, but also the neutron magnetic scattering function  $S(\mathbf{q}, \omega)$  may have most of its strength in inelastic channels.

In this paper we have assumed that the SDW  $\mathbf{Q}$ 's are commensurate and have values that coincide exactly with superstructure points in reciprocal space. We have also investigated the phonon spectrum if the  $\mathbf{Q}$ 's do not exact-

ly coincide. The cusps near  $\{100\}$  can still be explained, but only if  $|\mathbf{Q}|$  differs from the commensurate value by less than 1 or 2%.

#### ACKNOWLEDGMENTS

We are grateful to the National Science Foundation (Condensed-Matter Theory Section) for financial support.

- 
- <sup>1</sup>T. Toya, in *Lattice Dynamics*, edited by R. F. Wallis (Pergamon, New York, 1963), p. 91.
- <sup>2</sup>S. H. Vosko, R. Taylor, and G. H. Keech, *Can. J. Phys.* **43**, 1187 (1965).
- <sup>3</sup>W. A. Harrison, *Phys. Rev.* **139**, A179 (1965).
- <sup>4</sup>H. C. Gupta and B. B. Tripathi, *Phys. Status Solidi B* **45**, 537 (1971).
- <sup>5</sup>G. L. Krasko and Z. A. Gurskii, *Fiz. Tverd. Tela (Leningrad)* **13**, 2463 (1971) [*Sov Phys.—Solid State* **13**, 2062 (1972)].
- <sup>6</sup>J. Behari, *Philos. Mag.* **26**, 737 (1972).
- <sup>7</sup>C. M. Kachhava, *J. Phys. F* **3**, 24 (1973).
- <sup>8</sup>C. B. So and S. Wang, *J. Phys. F* **7**, 35 (1977).
- <sup>9</sup>M. A. Coulthard, *J. Phys. C* **3**, 820 (1970).
- <sup>10</sup>J. Hafner, *Phys. Lett.* **50A**, 271 (1974).
- <sup>11</sup>C. M. Bertoni, V. Bortolani, C. Calandra, and F. Nizzoli, *J. Phys. F* **4**, 19 (1974).
- <sup>12</sup>Ph. Schmuck and G. Quittner, *Phys. Lett.* **28A**, 226 (1968).
- <sup>13</sup>C. B. So, R. A. Moore, and S. Wang, *J. Phys. F* **8**, 785 (1978).
- <sup>14</sup>A. Sarkar, D. Sen, and S. Sengupta, *Pramana* **26**, 231 (1986).
- <sup>15</sup>Y. R. Wang and A. W. Overhauser, *Phys. Rev. B* **35**, 501 (1987).
- <sup>16</sup>E. R. Cowley, *Solid State Commun.* **14**, 587 (1974).
- <sup>17</sup>B. N. Brockhouse, T. Arase, C. Caglioti, K. R. Rao, and A. D. B. Woods, *Phys. Rev.* **128**, 1099 (1962).
- <sup>18</sup>J. R. Anderson and A. V. Gold, *Phys. Rev.* **139**, A1459 (1965).
- <sup>19</sup>A. W. Overhauser, *Phys. Rev. Lett.* **4**, 462 (1960).
- <sup>20</sup>A. W. Overhauser, *Phys. Rev.* **128**, 1437 (1962).
- <sup>21</sup>G. F. Giuliani and A. W. Overhauser, *Phys. Rev. B* **26**, 1671 (1982).
- <sup>22</sup>Y. R. Wang and A. W. Overhauser, *Phys. Rev. B* **35**, 497 (1987).
- <sup>23</sup>A. W. Overhauser, *Phys. Rev.* **167**, 691 (1968).
- <sup>24</sup>A. W. Overhauser, *Phys. Rev. B* **3**, 3173 (1971).
- <sup>25</sup>Y. R. Wang and A. W. Overhauser, *Phys. Rev. B* **34**, 8401 (1987).
- <sup>26</sup>B. G. Dick and A. W. Overhauser, *Phys. Rev.* **112**, 90 (1958).
- <sup>27</sup>C. A. Kukkonen and A. W. Overhauser, *Phys. Rev. B* **20**, 550 (1979).
- <sup>28</sup>J. Hubbard, *Proc. R. Soc. London Sect. A* **243**, 336 (1967).
- <sup>29</sup>R. Stedman, L. Almqvist, G. Nilsson, and G. Raunio, *Phys. Rev.* **163**, 567 (1967).
- <sup>30</sup>S. C. Ng and B. N. Brockhouse, *Solid State Commun.* **5**, 79 (1967).
- <sup>31</sup>S. C. Ng and B. N. Brockhouse, in *Neutron Inelastic Scattering* (IAEA, Vienna, 1968), Vol. 1, p. 253.
- <sup>32</sup>A. Furrer and W. Hälgl, *Phys. Status Solidi* **42**, 821 (1970).
- <sup>33</sup>A. W. Overhauser and L. L. Daemen, *Phys. Rev. Lett.* **61**, 1885 (1988).
- <sup>34</sup>B. J. C. van der Hoeven and P. H. Keesom, *Phys. Rev.* **137**, A103 (1965).
- <sup>35</sup>L. L. Daemen and A. W. Overhauser (unpublished).